



OPEN

Self-healing capacity of fiber-reinforced calcium phosphate cements

Anne V. Boehm¹, Susanne Meininger², Uwe Gbureck² & Frank A. Müller¹✉

A major problem concerning the mechanical properties of calcium phosphate cements (CPC) is related to their inherent brittleness, which limits their applicability to non-load bearing bone defects. In this work the preparation of a damage tolerant CPC is presented, where the incorporation of functionalized carbon fibers facilitates steady state flat crack propagation with crack openings below 10 μm . A subsequent self-healing process in simulated body fluid, that mimics the *in vivo* mineralization of bioactive surfaces, closes the cracks and completely restores the mechanical properties. Hereby, two pathways of self-healing are presented: i) intrinsic healing that bases on the inherent bioactive properties of the cement matrix and chemically treated fibers, and ii) capsule based extrinsic healing, where H_2PO_4^- is released as an initiator for the apatite formation. Such damage tolerant CPCs with self-healing capacity are of particular interest to increase the lifetime of implants as well as in the field of load-bearing bioceramics.

In millions of years, evolution developed materials with self-healing properties. These natural materials have the capability, to partially or completely restore in shape or function after the event of damage¹. In nature there are many familiar examples of self-healing that we take for granted, such as spontaneous healing of ruptured skin or mending of broken bones. Healthy human bone is a material that is permanently in change². Cells, osteoclasts and osteoblasts, respond to biomechanical stimuli and degrade or build bone accordingly, by using ions, such as calcium and phosphate that are present in the blood plasma as well as stored in already existing bones and teeth³. Due to these actions, a broken bone is able to mend.

In the recent 20 years, intense research on the development of self-healing materials was performed^{1,4,5}. Hereby, several strategies are to be distinguished. First of all, a distinction is made between autonomic healing, where no external trigger or action is required and non-autonomic healing, that presupposes external triggers. Furthermore, a differentiation is made between intrinsic healing, based on the inherent properties of the material, and extrinsic healing using external agents supplied in, for example, capsule systems⁶. Since polymers show chain mobility even at comparatively low temperatures, and a large number of chemical modification options are available, a multitude of self-healing mechanisms are found for this by far most intensively studied material class^{4,5,7–13}. Nevertheless, pathways for metals, ceramics and concretes were developed, as well^{12,14–16}. Many healing methods require external triggers, with temperature regimes being the most utilized⁵. In terms of extrinsic healing with capsule systems, the repeatability of the healing process is restricted¹. These factors can limit the fields of potential applications. However, applications with poor accessibility, for example in the construction industry or especially in clinical practice, particularly depend on self-healing materials, since here the replacement or even the detection of defects can be problematical. For clinical practice, numerous self-healing polymeric biomaterials and hydrogels were investigated and developed in the past 10 years^{9,13,17}. For brittle materials like cements or concrete the stabilization of the defect is essential for the healing strategy and can be achieved by different pathways¹⁸. In the case of concretes utilized for construction some systems with self-healing capability were developed. Hereby, different strategies were investigated with re-hydration, capsule systems or biological processes being most prominent¹². For the latter, bacteria are added to the cement system, which produce mineralization products closing the crack¹⁹. Defect stabilization and healing itself is typically based on the formation of salts in the crack, blocking of cracks with impurities or particles resulting from water infiltration or crack spalling, further hydration of unreacted cement or finally the expansion of cementitious matrix in the crack flanks¹⁵. Self-healing with apatite

¹Otto Schott Institute of Materials Research (OSIM), Friedrich Schiller University Jena, Löbdergraben 32, 07743, Jena, Germany. ²Department for Functional Materials in Medicine and Dentistry (FMZ), University of Würzburg, Pleicherwall 2, 97070, Würzburg, Germany. ✉e-mail: frank.mueller@uni-jena.de

materials was shown for apatite coatings and by utilizing phosphate-containing hydrogel in Portland cement paste^{20,21}.

To design a self-healing calcium phosphate cement (CPC) we suggest a mechanism with inspiration from self-healing mechanisms used for construction materials, utilizing crack stabilization and closing by damage tolerance and subsequent the formation of precipitate in the crack. Although both cements in the construction industry and CPCs, have to struggle with their brittle behavior and their poor accessibility in application in terms of self-healing, there are some very important differences in the challenge of designing a self-healing material. Besides others, the size of the components and workpiece differ and the choice of materials *in vivo* is limited to biocompatible ones. In general, CPCs result from the setting reaction of a calcium phosphate (CaP) powder and a liquid phase. Depending on the pH of the reaction either apatite or brushite is formed. However, in contrast to polymeric biomaterials or hydrogels this implant material, in clinical application since 1994 and under intense research for roughly 35 years by now, has significant advantages^{22–25}. Due to the paste-like state of CPC between mixing and setting, the cement can be injected and is therefore of particular interest in minimal invasive surgery²⁵. Beyond, the paste is capable to fill complex geometries and to ensure an intimate bone-implant-contact. Setting itself is an autonomous process, at moderate temperatures and without significant volume changes, which occurs *in vivo*²⁶. Thus, under physiological conditions the resulting precipitate, shows high chemical and structural similarity to mammalian hard tissue, that is composed of biological apatite²⁷. Finally, setting reactions at physiological temperatures allows the incorporation of drugs such as antibiotics, anti-inflammatory agents or growth factors in order to stimulate certain biological reactions²⁸. Beyond these advantages, however, CPCs are suffering from their inherent brittleness, which restricts their application²⁹. To overcome this drawback, damage tolerant systems were developed using, e.g. fiber reinforcement^{30–34}. Among others, carbon fibers (C-fiber) proved to be effective^{35–37}. In a previous study we investigated the influence of chemical fiber treatment on the mechanical performance of CPC³⁵. The bending strength of CPC was increased from 9 MPa to 19 MPa by adding 1 wt% untreated C-fibers. A chemical pretreatment of the C-fibers with *aqua regia* and calcium chloride lead to a further increase to 30 MPa. Additionally, the opening of occurring cracks was stabilized and fatal crack propagation was prevented, resulting in enhanced Work of fracture (WOF5). In addition to the tensile strength of the C-fibers, the surface chemistry of the fibers also influences the setting reaction of the CPC and thus the resulting matrix structure and strength. In the case of CPC with modified fibers, the fiber surface treatment increases the matrix fiber bond, leading to adhered matrix material that remains on the fibers surface after fracture. These remaining matrix particles impede the fiber pull-out, since they cause higher friction. Consequently, higher strength and WOF5 is observed for the composite³⁵.

In the present study, we go even further and present a self-setting, damage tolerant CPC with *in vitro* self-healing capability. For this purpose, an apatite cement with C-fiber reinforcement was damaged in a controlled manner and healed in simulated body fluid (SBF). Since SBF mimics the composition of the inorganic part of human blood plasma, it can reproduce the *in vivo* formation of apatite on bioactive surfaces and is therefore used to investigate the *in vitro* bioactivity^{38–40}. In this context, a surface is considered to be bioactive, if it facilitates the heterogeneous nucleation and growth of apatite^{41,42}. Combining the *in vitro* ability of SBF to form apatite with a damage-tolerant bioactive material, the aim of the present study is to design a cement-based implant material with an intrinsic self-healing capacity, where cracks are instantly healed by a biomimetic mineralization process. Beyond, also an extrinsic healing pathway will be investigated, using H_2PO_4^- supplying capsules, which trigger the precipitation of CaP. Such self-healing CPC are of potential interest for load-bearing orthopedic applications, since occurring cracks might be filled with new bone instead of leading to catastrophic *in vivo* failure.

Materials and Methods

The experimental procedure for sample preparation and self-healing tests is schematically illustrated in Fig. 1. As indicated on the left, the CPC samples were prepared as a composite of C-fibers embedded in an α -tricalcium phosphate (α -TCP) matrix. Partly sodium dihydrogen phosphate (NaH_2PO_4) capsules were added to enable extrinsic healing experiments. Besides other tests, self-healing was examined regarding to the regime presented on the right in Fig. 1. In the following chapters, the single parts of the experimental procedure are described in detail.

Cement preparation. α -TCP was prepared by sintering calcium hydrogen phosphate (CaHPO_4 , Mallinckrodt-Baker, Germany) and calcium carbonate (CaCO_3 , Merck, Germany) in a molar ratio of 2:1 for 5 h at 1400 °C followed by quenching to room temperature. The sintered cake was crushed and passed through a 125 μm sieve followed by ball milling at 200 rpm for 4 h⁴³. A solution of 1 M trisodium citrate ($\text{Na}_3\text{C}_6\text{H}_5\text{O}_7$, Carl Roth, Deutschland) and 2.5 wt% disodium hydrogen phosphate (Na_2HPO_4 , Carl Roth, Deutschland), prepared with demineralized water, served as liquid phase in the cement preparation.

C-fibers (Nippon Graphite Fiber Corporation, Japan) with a diameter of $d = 7 \mu\text{m}$ were cut to a length of 1 cm before desizing twice in boiling isopropanol (Carl Roth, Germany). Subsequently, the fibers were dried in a freeze dryer and processed as they are or stirred for 40 min in *aqua regia* (HCl, Carl Roth, Germany and HNO_3 , Carl Roth, Germany), washed with water and stored in 1 M calcium chloride (CaCl_2 , VWR Chemicals, Belgium) solution for 1 day, as reported in detail previously³⁵. After the modification the C-fibers were freeze-dried.

To prepare capsules $\text{NaH}_2\text{PO}_4 \cdot 2 \text{H}_2\text{O}$ (VWR Chemicals, Belgium) salt was coated with Degacryl (PMMA, 15 kDa, Evonik Industries AG, Germany) dissolved in acetone using a fluidized bed coating (Mini Glatt 12104, Glatt, Germany). Particle size and surface ratio were estimated by analyzing light microscopic images of NaH_2PO_4 capsules and cement fracture surfaces using the software ImageJ. Light microscopy (Axio Vision, Carl-Zeiss, Germany) was performed in light field using z-stack.

α -TP, 1 wt% C-fibers, and optionally 2 wt% NaH_2PO_4 , according to the compositions listed in Table 1, were mixed in dry state by hand and combined with the liquid phase at a powder-to-liquid ratio (PLR) of 3 g·mL⁻¹. The

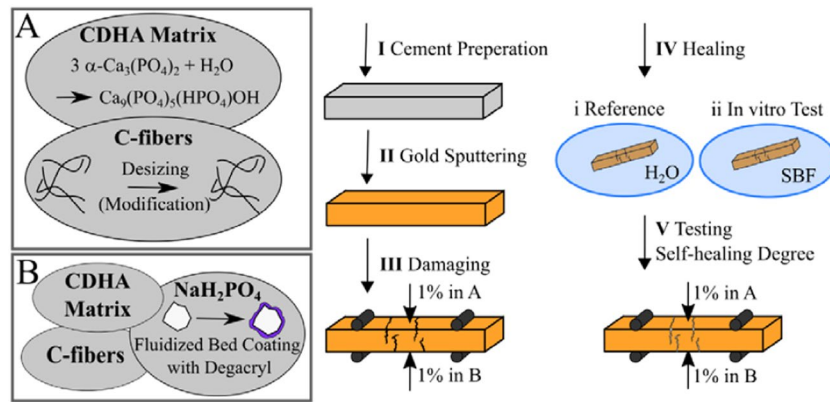


Figure 1. Sample preparation and regime of self-healing tests. The left part illustrates the two examined cement systems, (A) calcium deficient hydroxyapatite (CDHA) matrix and C-fibers as well as (B) CDHA matrix, C-fibers and NaH_2PO_4 supply, whereas on the right the procedure for self-healing tests with the steps I to V is schematically visualized.

Sample	Fiber Additive	Capsule Additive
CPC	—	—
C-CPC	1 wt% untreated C-fibers	—
C_m -CPC	1 wt% <i>aqua regia</i> and CaCl_2 treated C-fibers	—
PO_4 -C-CPC	1 wt% untreated C-fibers	2 wt% NaH_2PO_4 capsules
PO_4 - C_m -CPC	1 wt% <i>aqua regia</i> and CaCl_2 treated C-fibers	2 wt% NaH_2PO_4 capsules

Table 1. Sample composition and nomenclature.

mixed CPC pastes were transferred into silicon molds and stored at high humidity and 37 °C for 4 h. Then they were stored to demineralized water for final setting at 37 °C for 7 days. Hereby, 40 g α -TCP and the corresponding amounts of additives were used to obtain 32 samples, 16 of which were each tested with similar parameters (e.g. 16 reference in water and 16 immersion in SBF for specific time). After setting in demineralized water for 7 days, CPCs were ground plane-parallel using abrasive paper up to a grit of 1000.

Applying the Gilmore needle test, the initial (needle diameter 2.12 mm, weight 113 g) and final (needle diameter 1.06 mm, weight 454 g) setting time was estimated using plate specimens with a diameter of 20 mm.

Mechanical properties and self-healing capacity. The mechanical properties of CPC were characterized using a universal testing machine (Z2020, Zwick, Germany). In three-point bending tests specimens with dimensions of length $l = 30$ mm, height $h = 3$ –4 mm and breadth $b = 6$ mm were tested applying a support span of $L = 20$ mm, a loading rate of $1 \text{ mm} \cdot \text{min}^{-1}$, and a preload of 0.1 N. The bending stress σ_b was calculated according to Eq. 1, with the force F . The strain ε_b was calculated according to Eq. 2 with the deflection s . Additionally, the Work of fracture up to a strain of 5% $WOF5$ was calculated according to Eq. 3. Hereby the force F was integrated over the deflection s from $s_0 = 0$ to the deflection s_5 , where ε_b equals 5%. Although samples show much higher strain at failure, the residual strength at higher strain strongly depends on fiber orientation, causing the error being vast. Since 5% strain is closer to the actual strain of bone⁴⁴ this limit was chosen for a better comparability also concerning clinical applications.

$$\sigma_b = \frac{3FL}{2bh^2} \quad (1)$$

$$\varepsilon_b = \frac{6sh}{L^2} \cdot 100\% \quad (2)$$

$$WOF5 = \frac{\int_{s_0}^{s_5} Fds}{bh} \quad (3)$$

For the test of the self-healing capacity the steps I to V, shown in Fig. 1 were applied. Hereby each test was performed with $n = 16$ specimens. (I) Samples were prepared according to the cement preparation procedure and dried after preparation. (II) Cement bars were sputtered with gold, which is bio-inert, to ensure that a

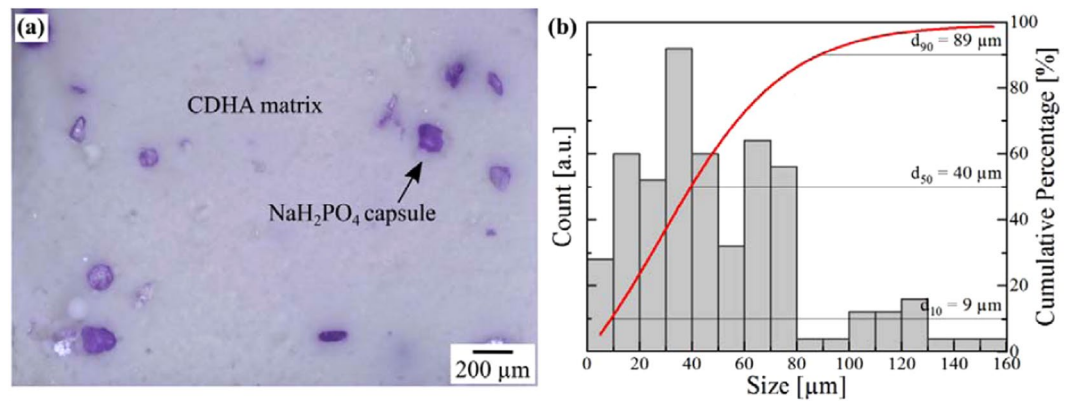


Figure 2. (a) Fracture surface of $\text{PO}_4\text{-CPC}$ showing capsules distribution as well as (b) size distribution of NaH_2PO_4 capsules.

mineralization is directed to freshly formed defects. (III) Subsequently, the specimens were damaged in a controlled manner by measuring the bending stress up to an elongation of 1% in both directions A and B one after the other by turning the sample. 1% strain was chosen, since the strain at maximum bending strength is in this range and a reduction of strength upon second loading without healing is measurable. (IV) Samples were stored for 7 days in either SBF or demineralized water at 37 °C. SBF solutions with ionic concentrations almost equal to the inorganic part of human blood plasma were prepared according to Müller *et al.*³⁸ Hereby the immersion volume was 200 mL. (V) After rinsing with demineralized water and drying, the bending stress up to a strain of 1% was measured in both directions in the same order as previously. The degree of self-healing *SHD* is defined as the sum of strengths in both directions A and B after storage σ_{bA}^* and σ_{bB}^* , divided by the sum of strengths before healing σ_{bA} and σ_{bB} , Eq. 4.

$$SHD = \frac{(\sigma_{bA}^* + \sigma_{bB}^*)}{(\sigma_{bA} + \sigma_{bB})} \cdot 100\% \quad (4)$$

Healing kinetics were measured mechanically, applying the above described regime for healing periods of 1, 3, 5 and 7 days, respectively. Beyond, the composition of SBF was measured everyday by taking 5 mL from the solution. 5 mL of 20 vol% HNO_3 were added and the solution was passed through a syringe filter with a pore size of 0.45 μm . The concentration of calcium and phosphor was quantified using a simultaneous radial ICP-OES spectrometer 725ES (Agilent, Waldbronn, Germany) with a CCD-detector. For these tests the immersion volume was raised to 250 mL without further refilling. On the basis of the results of the kinetic measurements, cyclic healing in SBF was performed using a healing period of 5 days for three cycles by repeating steps III to V. Scanning electron microscopy (SEM, Sigma VP, Carl-Zeiss, Germany) on reinforced and healed CPC was performed after 7 days of (I) setting or (V) healing and subsequent drying.

Statistical analysis. The self-healing capacity in terms of *SHD* was analyzed for significant differences between groups by one-way ANOVA using both the comparison with the respective reference in water and the differences between the healed samples. For all tests the level of significance was set at $p < 0.05$.

Results

Cement characteristics and mechanical properties of CPC. In this study, the self-healing of cements reinforced with C-fibers and to which additional NaH_2PO_4 capsules were optionally added was investigated. Whereas the properties of C-fibers reinforced CPC were already published in a previous study³⁵, the characteristics of the capsules and their influence are reported in the following. The capsules consist of a NaH_2PO_4 salt, which was coated with the purple stained polymer Degacryl, which is based on PMMA. The capsules are evenly distributed in the cement and have a surface ratio of $7\% \pm 3\%$ at the fracture surface (Fig. 2a). The size distribution of the irregularly shaped NaH_2PO_4 capsules displays a broad distribution with a d_{50} of 40 μm (Fig. 2b).

The X-ray diffraction in Fig. 3 shows, that in all systems a cement matrix consisting of calcium deficient hydroxyapatite (CDHA) is formed in a setting process from the raw powder $\alpha\text{-TCP}$ and an aqueous solution. The diffraction patterns show the presence of two phases, Hydroxyapatite (HAp) and $\alpha\text{-TCP}$. The Rietveld analyses presented in Table 2 revealed that for CPC without additives the content of $\alpha\text{-TCP}$ is highest at 13%, while the addition of both fibers and NaH_2PO_4 capsules leads to a reduction of the $\alpha\text{-TCP}$ content to 9% and 5%, respectively.

Figure 4a illustrates the resulting morphology of the CPC matrix without further additives. It consists of CDHA crystals, which form a porous network. The initial and final setting time for pure CPC was estimated as $t_i = 25$ min and $t_f = 105$ min and shows upon fiber addition a significant reduction³⁵. This effect was even more pronounced, when PO_4^{3-} capsules were added in the $\text{PO}_4\text{-C}_m\text{-CPC}$ system, where the setting times are reduced to $t_i = 13$ min and $t_f = 21$ min. Beyond, the addition of capsules led to a smaller crystal size (Fig. 4b).

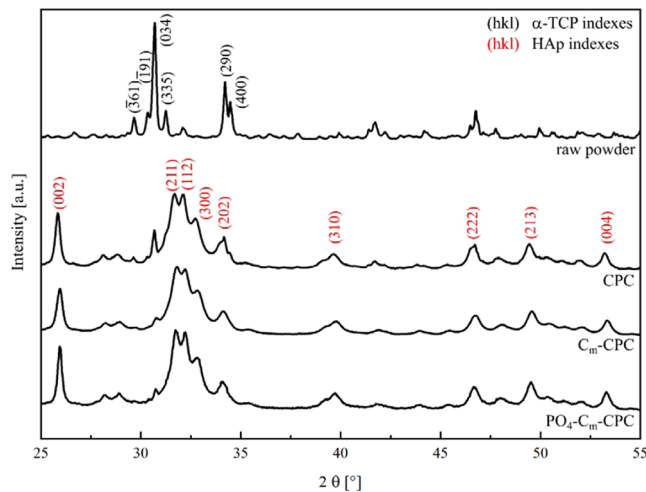


Figure 3. X-ray diffraction analyses of the raw powder, CPC, C_m -CPC and PO_4 - C_m -CPC after 1 week setting in demineralized water.

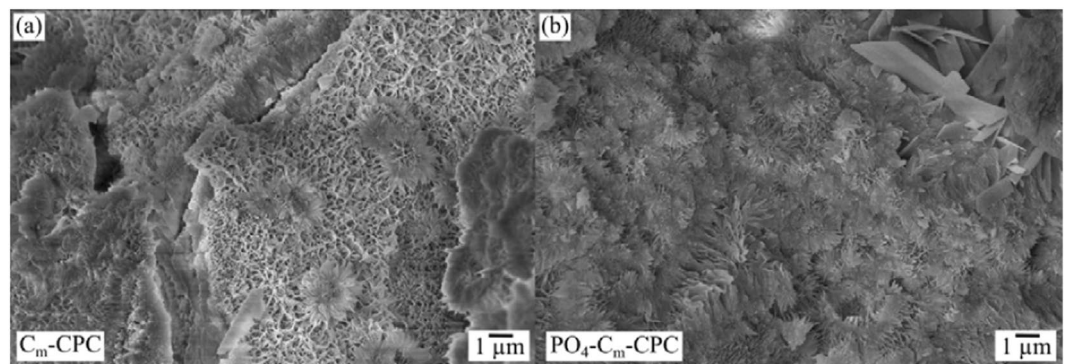


Figure 4. Scanning electron microscopy of fracture surfaces, showing (a) C_m -CPC and (b) PO_4 - C_m -CPC.

Sample	α -TCP [%]	HAp [%]	Rwp
α -TCP	100	—	4.612
CPC	13	87	8.067
C_m -CPC	9	91	8.043
PO_4 - C_m -CPC	5	95	8.800

Table 2. Phase quantification from XRD using Rietveld.

During the mixture, some of the capsules tear apart and release $H_2PO_4^-$, causing a higher local saturation and consequently an accelerated nucleation. Thus, the crystal size is reduced, also resulting in altered mechanical behavior (Table 3). The incorporation of capsules increased the bending strength by 100% when untreated fibers were used and by 50% when chemically pretreated fibers were used. Besides the increase of strength, all reinforced cements show enhanced damage tolerance in comparison to pure CPC. Hereby, the $WOF5$ was enhanced from $0.02 \text{ kJ}\cdot\text{m}^{-2}$ for pure CPC to $1.9 \text{ kJ}\cdot\text{m}^{-2}$ in the case of C_m -CPC³⁵. Upon the addition of PO_4 -supply, $WOF5$ remained in the same range with $WOF5 = 1.7 \text{ kJ}\cdot\text{m}^{-2}$ for both, PO_4 -C-CPC and PO_4 - C_m -CPC.

The damage tolerance of the reinforced systems is caused by changes in the cracking behavior (Fig. 5). Whereas for CPC only one single crack with a fatal crack opening propagation is observed, the fiber reinforcement leads to multiple cracking and a crack stabilization with crack openings below $10 \mu\text{m}$. Thus, the damage tolerance can be assumed for all fiber reinforced CPC-systems shown in this study.

Self-healing capacity. The self-healing capacity of cements was proven by the mineralization-induced closure of cracks and a recovery of their mechanical properties, respectively. The comparison of the stress-strain curves for CPCs prior and after immersion shows self-healing for all samples in SBF and for CPCs with capsules also in water. Since the bending tests were applied only up to a strain of 1% and in both directions, the individual

Sample	Initial Setting Time [min]	Final Setting Time [min]	Bending Strength [MPa]	Work of Fracture to ϵ_0 , 5% [$\text{kJ}\cdot\text{m}^{-2}$]	Degree of Self-Healing in SBF [%]
CPC	25.0 ± 0.5	105 ± 5	9.2 ± 1.7	0.02 ± 0.004	0
C-CPC	20.0 ± 0.5	65 ± 2	19.3 ± 1.9	0.7 ± 0.4	102 ± 18
C_m -CPC	18.5 ± 0.5	50 ± 2	30.3 ± 2.8	1.9 ± 0.3	107 ± 55
PO_4 -C-CPC	16.0 ± 0.5	25 ± 1	37.8 ± 4.2	1.7 ± 0.6	110 ± 17
PO_4 - C_m -CPC	13.0 ± 0.5	21 ± 1	45.0 ± 3.8	1.7 ± 0.5	110 ± 8

Table 3. Setting and mechanical properties of CPCs as well as *SHD* after immersion for 7 days in water. Listed values are mean \pm standard variation. Data of setting and mechanical properties of CPC, C-CPC and C_m -CPC are captured from previous study³⁵.

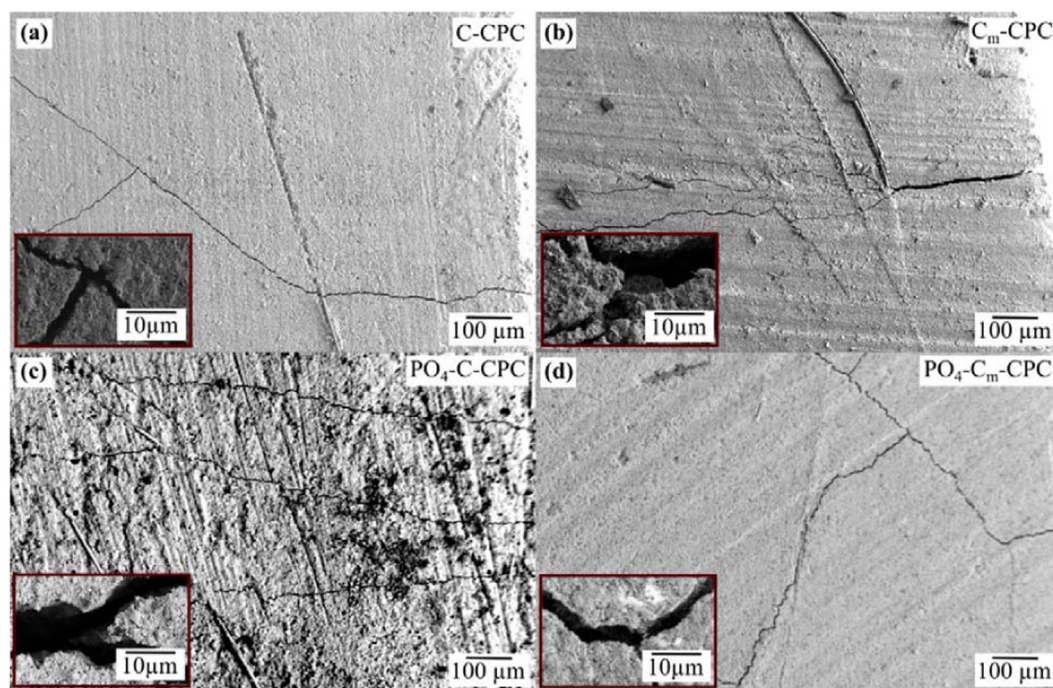


Figure 5. Crack propagation and detailed view after 3-point bending of (a) C-CPC, (b) C_m -CPC, (c) PO_4 -C-CPC and (d) PO_4 - C_m -CPC. Scanning electron microscopy was performed on the lateral surfaces between the pressure points.

measurements are not significant for the mechanical properties of the material, but the relation of strength from first measurement to second measurements reflects the self-healing capability of the CPCs. Exemplarily, stress-strain curves for C_m -CPC at first and second loading stored for 7 days in water and SBF, respectively, are shown in Fig. 6. Hereby, not only the maximum strength, but also the similar slope in the case of samples stored in SBF implicates the self-healing of CPCs. However, while individual maxima are visible at the first load, the stress increases more continuously with strain at the second load.

Figure 7a shows the SEM image of a C_m -CPC after self-healing, reflecting the damaging-healing-damaging process. In composites consisting of a CDHA matrix (light grey) reinforced with chemically treated C-fibers, defects were introduced by straining. These defects healed during exposure to SBF by a mineralization within the crack. The mineralization product can be distinguished by its darker grey color. In the detailed view of the healed crack a porous plate-like morphology of the precipitate can be observed (Fig. 7b). It can also be seen that the crack propagating from the left splits into two, both of which are mineralized. When the strength was examined again after self-healing, the healed crack is reopened. Contrary to the previous course, this time, however, the crack did not split, but ran exclusively along the upper line. A similar cracking pattern can be observed in the case of PO_4 - C_m -CPC shown in Fig. 7c,d. For this particular crack, which was formed during the first loading, the closure occurred during immersion in SBF. At the second loading, the crack was reopened, with the crack running through the mineralized crack filling. Figure 7e quantifies the self-healing capacity of C-CPC, PO_4 -C-CPC, C_m -CPC and PO_4 - C_m -CPC. In general, both plots show a similar course. However, as mentioned earlier, but not obvious in the boxplots due to the normalization in the formula of the self-healing degree *SHD*, the absolute strength of the cements strongly differs. Damaged C-CPCs did not recover when stored in water but reached only 60–80% of their original strength (Fig. 7e). On the contrary, when analogous C-CPCs were stored in SBF

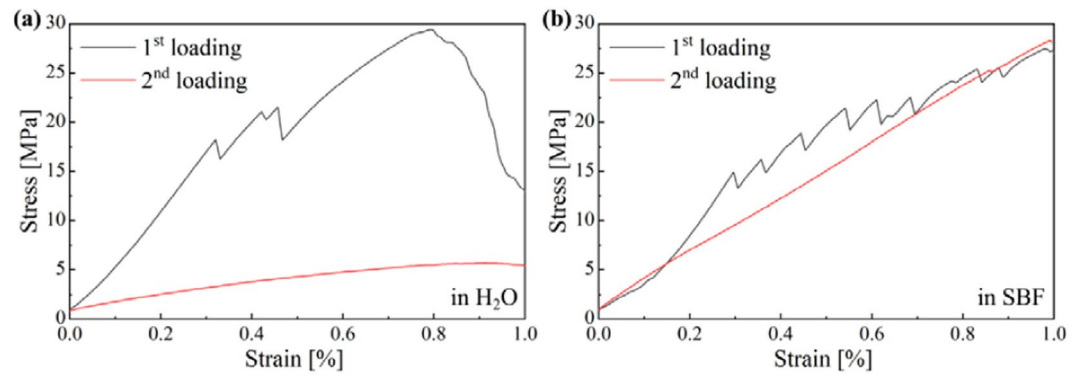


Figure 6. Stress-strain curves of C_m -CPC showing first loading (black) and second loading (red) during self-healing tests for samples stored 7 days in (a) water and (b) SBF.

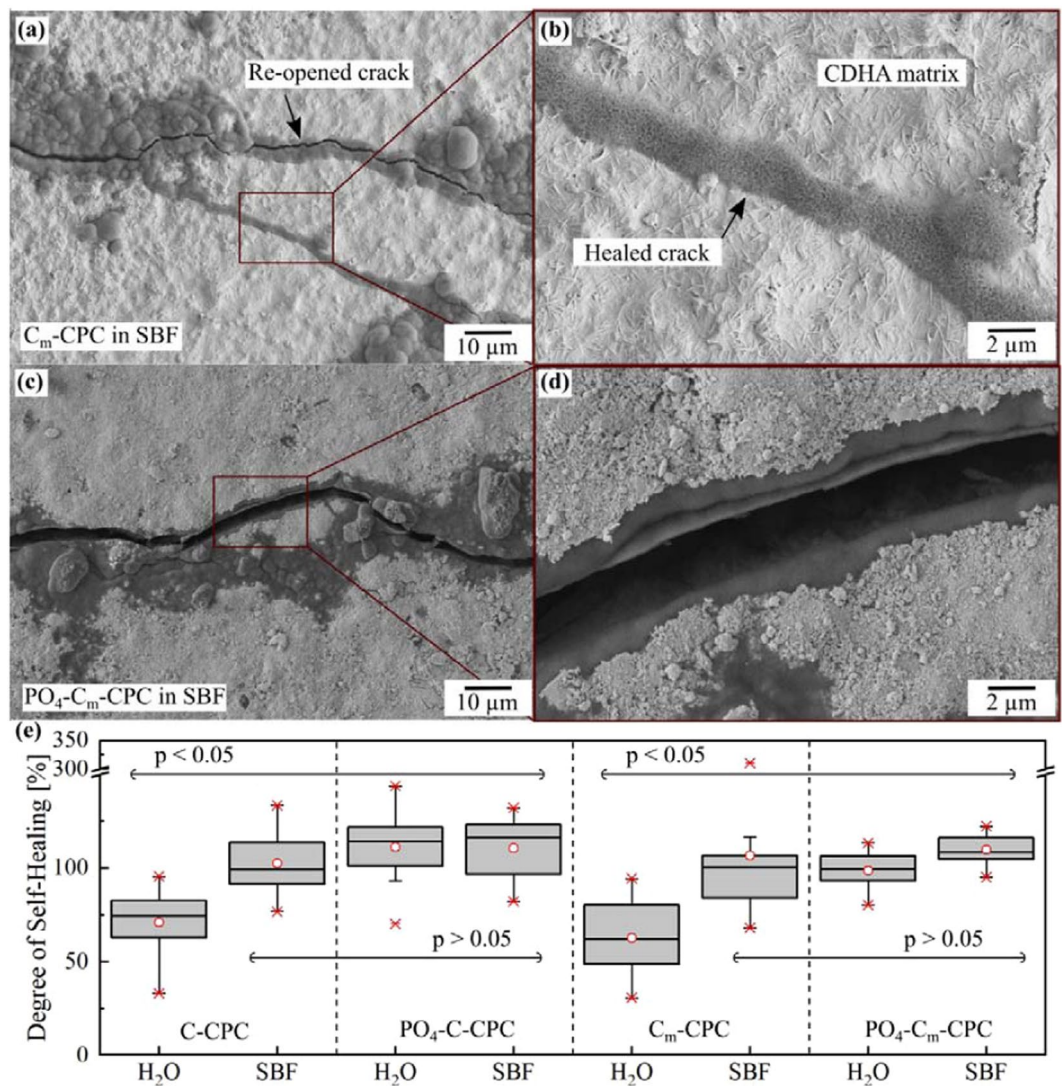


Figure 7. SEM images of a C_m -CPC that was damaged, healed and again damaged in (a) overview and (b) a detailed view of the mineralization in the crack, as well as for PO_4 - C_m -CPC with similar regime in (c) and (d). Scanning electron microscopy was performed on the side surfaces between the loading bars. Self-Healing capacity in terms of mechanical properties after 7 days storage in water or SBF of (e) C-CPC as well as PO_4 -C-CPC, and C_m -CPC as well as PO_4 - C_m -CPC. Results from ANOVA are indicated with $p < / > 0.05$.

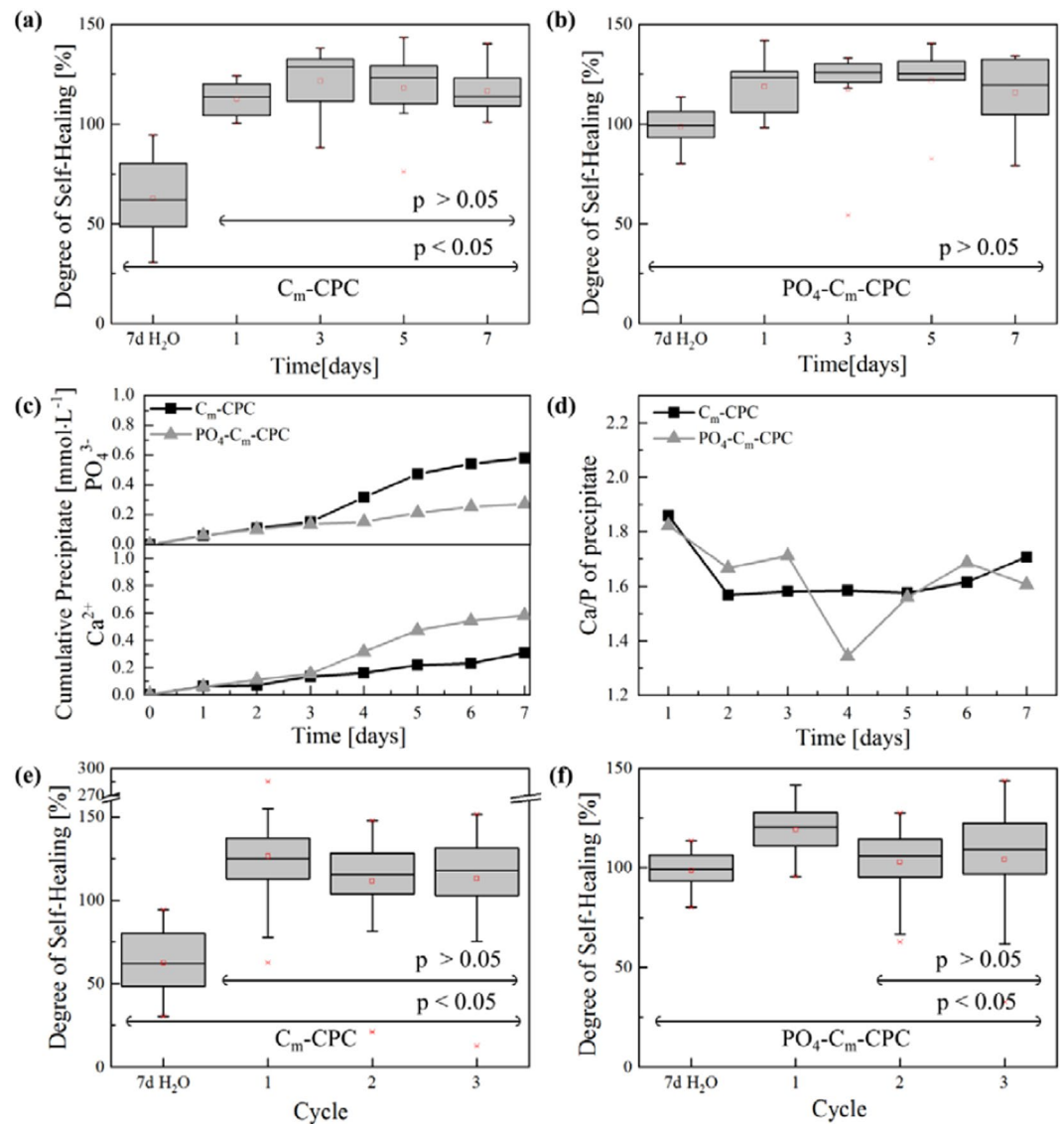


Figure 8. Kinetic study of C_m -CPC and PO_4 - C_m -CPC (a,b) with respect to *SHD* as a function of healing time and ICP-OES analyses of the SBF composition during healing showing (c) the cumulative precipitation of Ca^{2+} and PO_4^{3-} and (d) the calcium-phosphor ratio. The measurement error for cumulative precipitate is about 1%. Repeatability of self-healing for C_m -CPC and PO_4 - C_m -CPC (e,f) shows *SHD* for different cycles of self-healing. The self-healing was tested in SBF. Results from ANOVA are indicated with $p < /> 0.05$.

an average *SHD* of 102% was observed. A similar increase in *SHD* was also detected for C_m -CPC (Fig. 7e). Here, the reference in water shows about 63% in the second test of the mechanical properties, while the healing in SBF causes an average restoration of *SHD* of 106%. The addition of capsules changed the healing behavior particularly in water, where *SHD* reached 110% and 98% for untreated and modified fibers, respectively (Fig. 7e).

Figure 8 illustrates the healing kinetics and repeatability for C_m -CPC and PO_4 - C_m -CPC. Measurements of the mechanical recovery in dependence of time revealed the beginning of healing at day one with statistical significance ($p < 0.05$) (Fig. 8a,b). Hereby, only negligible differences were observed in the average *SHD* over the time period of 7 days ($p > 0.05$). Analyses of the amount of precipitate from the media are shown in the Figure 8c and reveal a precipitation over the whole time period. Slight differences between C_m -CPC and PO_4 - C_m -CPC are noted by the increased concentration of PO_4^{3-} in solution for PO_4 - C_m -CPC. Fig. 8e,f demonstrate the repeatability of self-healing for C_m -CPC and PO_4 - C_m -CPC. Self-healing was proven for C_m -CPC over three cycles without significant efficiency loss ($p > 0.05$), whereas a significant decrease in *SHD* from cycle 1 to 2 was observed for PO_4 - C_m -CPC ($p < 0.05$), whereas to cycle 3 no further decrease was detectable ($p < 0.05$).

Figure 9 shows a crack in a C_m -CPC during closure *via* mineralization. An overview of the crack is given in Fig. 9a, which shows mineralization and crack bridging at several points. In the detail view in Fig. 9b one particular spot is magnified, exposing a sheared α -TCP grain with mineralization at its surface. The mineralization product, similar to the previously shown results, is of porous nature and consists of needles.

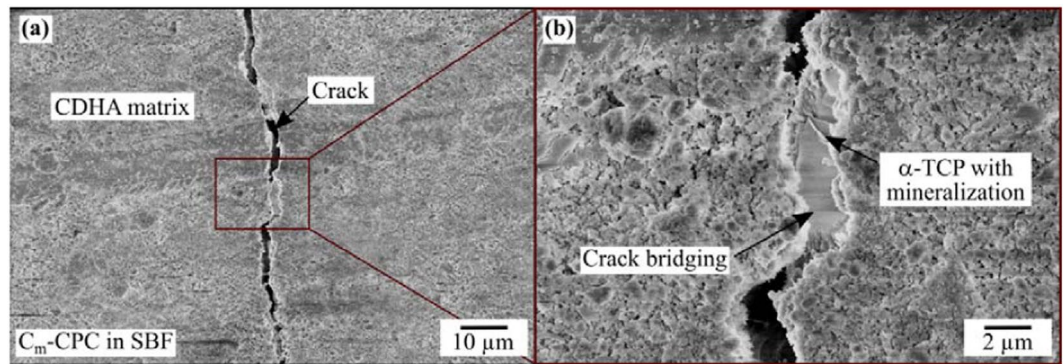


Figure 9. SEM of a C_m -CPC after immersion in SBF showing incomplete filling of a crack in (a) overview and (b) detailed view with an α -TCP grain in the crack.

Discussion

The self-healing capacity of damage tolerant CPC reinforced with C-fibers has been successfully demonstrated through an intrinsic as well as extrinsic mechanism. The damage tolerance results in crack stabilization, which is seen as a prerequisite to gain time for a subsequent healing process. The healing itself was achieved by the mineralization of cracks in SBF, mimicking the inorganic composition of human blood plasma. After a setting time of 7 days for all samples, the matrix mainly consisted of CDHA with a low content of α -TCP (Fig. 3). The addition of both C-fibers and capsules led to a reduction of the α -TCP amount (Table 2). The use of C-fiber reinforcement with both, untreated (C-CPC) and *aqua regia*/CaCl₂ treated fibers (C_m -CPC), respectively, lead to a significant increase of strength³⁵. Changes during the setting of the cement, which are shown both in setting times and in phase analyses of the cements, as well as negatively charged surface groups on the fiber led to strong fiber-matrix interactions, which resulted in an altered fracture behavior³⁵. This finally contributed to fulfilling our first requirement of effective bridging and thus stabilization of cracks. The additional incorporation of capsule system, consisting of polymer coated NaH₂PO₄ salt crystals (PO₄-C-CPC and PO₄- C_m -CPC), lead to a further increase of strength, due to changes in the cement setting kinetics (Table 3). Since some of the NaH₂PO₄ salt is exposed during mixing due to rupture of the coating, both, the subsequently reduced pH of the paste and the oversaturation with H₂PO₄⁻ most likely accelerate the nucleation of calcium phosphate phases such as brushite, octacalcium phosphate or amorphous calcium phosphate, which transform into CDHA when the pH increases to a physiological level. As a result, the CPC matrix consists of smaller crystals (Fig. 4). It is well known that the crystal size has a strong influence on the mechanical properties, whereby smaller crystals can result in higher strength due to their more effective energy dispersion⁴⁵. Beyond, it was shown that the C-fiber reinforcement causes multiple cracking. While in a standard CPC one crack would open and propagate catastrophically, here several cracks are opened, and the energy is dissipated by fiber-matrix interactions, resulting in steady state crack propagation with narrow crack openings below 10 μ m (Fig. 5). This damage tolerance due to fiber incorporation can also be seen by the drastic increase of WOF5 (Table 3). Whereas pure CPC shows a negligible WOF5 of 0.02 kJ·mm⁻², the fiber incorporation of untreated or chemically modified fibers causes an increase of WOF5 by a factor of 35 and 95, respectively³⁵. Beyond the effect of fiber reinforcement, also the influence of the H₂PO₄⁻ supply was investigated. As mentioned earlier, partial release of H₂PO₄⁻ results in a smaller crystal size of the CDHA matrix and therefore a more effective crystal interlocking and energy dissipation. Consequently, also PO₄- C_m -CPC shows multiple cracking with narrow openings. This effect is not only showing in enhanced strength, but also in a WOF5 of 1.7 kJ·mm⁻². As a result of these cracking processes all of the investigated CPC systems are damage tolerant. Besides the damage tolerance, crack stabilization at narrow openings is also believed to be essential for a successful mineralization of the cracks for self-healing of the CPCs, since mineralization processes are time consuming and the thickness of mineralized layers depends on time⁴⁶. On a bioactive surface exposed to SBF mineralization is observed within a few days, as schematically illustrated in the detail views of Fig. 10. Hereby, a charged surface attracts oppositely charged ions from solution and the nucleation of a calcium phosphate is initiated^{47,48}. In the further process, a biomimetic apatite layer consisting of small platelet shaped crystals is formed³⁸. In the present system, the CPC matrix that consists of CDHA crystals acts as bioactive surface, attracting Ca²⁺ and PO₄³⁻ ions from solution⁴⁹. As a result, biomimetic apatite nucleates and grows (Fig. 7a,b). Beyond that, the chemically treated fibers can act as additional nucleation sites, either due to their negative surface charge or, due to matrix material present on the fibers surface after fracture. Hereby, the microstructure of the matrix might also influence the bioactivity, since with a higher specific surface also more nucleation sites are present⁵⁰. In addition to the bioactivity of the crack surfaces and the fibers, however, the ion supply, especially PO₄³⁻, also limits the mineralization rate⁵¹. A second pathway to mineralization is observed in the case of additional NaH₂PO₄ capsules in the composite. Here, the crack most likely induces mechanical rupture of the polymer coating and a subsequent dissolution of the salt. As a result, a local H₂PO₄⁻ oversaturation in the direct surrounding of the capsule occurs, causing the precipitation of a CaP and the storage at physiological pH in SBF or water leads to the formation of apatite. Examination of the surface ratio of capsules on the fracture surface of CPC revealed a content of 7%, which is exposed and presumably ruptured due to crack propagation. Therefore, a capsule-based extrinsic initiation of mineralization is most probable. The mineralization independent on whether it is initiated by active crack flanks, fiber coatings or a capsule induced oversaturation, causes in a first instance a shortening and narrowing of

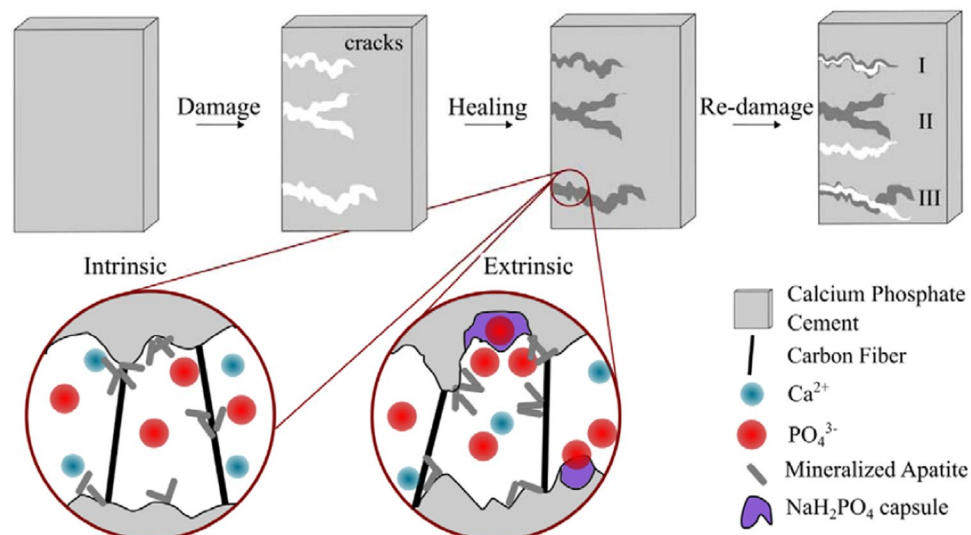


Figure 10. Self-healing and re-damage mechanisms of CPC with visualization of possible crack paths (I-III) during re-damage.

the crack, which overall reduces the defect size. Additionally, due to mineralization sites along the crack surface such as fibers or capsules, a bridging effect can occur. In this process, the precipitation closes the crack at certain points, which on the one hand stabilizes the crack and on the other hand splits the crack (Fig. 9). This shielding can be expected to reduce the size of defects, which according to Griffith directly affects the strength and thus leads to the restorage of the mechanical properties (Fig. 7c,d)⁵². Additionally, beyond the relation of the maximum strengths in first and second loading, also similarities in their slopes indicate the self-healing of the CPCs (Fig. 6). The exemplary curves show a steep slope and isolated drops for samples during the first loading. Hereby the drops are caused by crack opening followed by an increase due to the stabilization by fibers. Upon second loading, for samples stored in water the slope and maximum strength are dramatically decreased, whereas after storage in SBF both, the maximum strength as well as the slope are very similar to the first loading. The absence of individual steps may indicate that similar cracks are reopened. Since the slope and strength are nevertheless similar, a possible conclusion might be, that although crack opening is facilitated due to changes in the sample surface, the crack propagation through the materials volume is similar to undamaged CPC. In addition to crack healing, some *SHD* have average values exceeding 100%, which would correspond to a strengthening of the cement. The strength of ceramics is determined by the distribution of defects and their size. The smaller and less defects are present, the stronger is the material, since flaws initiate the propagation of cracks^{53,54}. Thus, the presented healing mechanism is not limited to newly formed defects by e.g. loading, but also affects pre-existing ones. As a result, the overall defect size is reduced, resulting in higher strength. This also affects the crack formation upon second loading of a healed sample. Several events are conceivable, as schematically illustrated in Fig. 10. Either (I) the initial crack is re-opened and the propagation takes place along the same path, or (II) new cracks at different positions are opened. Beyond, (III) variations from the crack course might occur. Hereby, the change of crack geometry by mineralization is decisive. Mineralization itself depends amongst others on the ion-supply as well as on the presence of nucleation sites. These parameters are influenced by the porosity and the direct surrounding of the defect. In the case of cracks, the perfusion is ensured and even supported by capillary forces, whereas in the case of pre-existing defects the porosity is determining and perfusion can be impeded. Hence, the successful healing of pre-existing or newly formed defects strongly depends on the direct surrounding and which mechanism of re-damage is activated. If a crack is not completely filled, or no other defects are present, the re-opening of the crack is most likely. On the contrary, a fully mineralized crack increases the probability for the formation of new cracks starting at different defects. Finally, inhomogeneities in the filling might lead to a change of the crack pathway. In particular, this is likely, if the fiber stabilization leads to variations of the crack opening during its propagation.

The mineralization itself is a continuous process, that was investigated kinetically for C_m -CPC and PO_4 - C_m -CPC in terms of mechanical restoration and time dependent analyses of the healing media (Fig. 8). Here, the mechanical characterization revealed that even for a low amount of precipitate from solution, the healing occurred instantly. Since, the defect size is essential for crack propagation, even a low degree of mineralization might have an enormous impact on the defect size by shielding of cracks and consequently on the mechanical properties. In the course of the healing process, the degree of mineralization from solution increases. After one day a fast decline of Ca^{2+} concentration is observed, resulting in a high calcium-phosphor ratio (Ca/P) ratio of 1.9. This is in agreement with the described mineralization mechanism of biomimetic apatite on synthetic apatite⁵⁵. Besides, less time is observed in the case of the PO_4 - C_m -CPC. This indicates, that initially the capsule material is dissolved and precipitated, before ions are consumed from the SBF. However, the release and adsorption processes of the CPC matrix material impede the interpretation of the precipitation processes from the SBF,

which makes it difficult to interpret the ICP-OES results. Since the matrix material consists of CDHA it has an inherent driving force to attract Ca^{2+} from solution due to the presence of calcium voids in the crystal lattice. On the contrary, it was shown in a previous study, that CDHA cements release phosphate ions³⁵. This could also be responsible for the higher Ca/P ratio, which is typically around 1.5 for biomimetic apatite⁵⁵. Nevertheless, since the ICP results are in accordance with the mechanical characterization of healing in water for $\text{PO}_4\text{-C-CPC}$ and $\text{PO}_4\text{-C}_m\text{-CPC}$, participation of capsule material in the mineralization process can be assumed. It is believed that the dissolution of the encapsulated salt in combination with a setting of unreacted powder present in the CPC or ion release from the matrix, initiates mineralization and hence healing. The repeatability of the self-healing was tested for both $\text{C}_m\text{-CPC}$ and $\text{PO}_4\text{-C}_m\text{-CPC}$ with healing periods of 5 days. Self-healing over three cycles is verifiable with *SHD* exceeding 100% for both, extrinsic and intrinsic healing (Fig. 8e,f). Since healing is based on mineralization from SBF and inherent crack stabilization, the healing process is efficient as long as the ion supply is assured. This distinguishes our extrinsic self-healing mechanism from most systems known in literature. Usually, extrinsic healing is only possible once, because no healing agent is available for further cycles⁵. In our presented case, intrinsic self-healing dominates, when the healing agent is consumed. This assumption is supported by a slightly reduced healing efficiency from the first to the second cycle from 119% to 103% with statistical significance ($p < 0.05$), while no further change could be detected in the third cycle.

However, *in vivo* some significant differences to our *in vitro* model are expected. First of all, instead of the static presence of the liquid, a perfusion with human blood is expected, enhancing the ion supply and accelerating the mineralization rate⁵⁶. Nevertheless, besides the inorganic components of SBF, also organic ones e.g. proteins, are present *in vivo* which can decelerate the formation of apatite⁵⁷. Therefore, we suspect, that the kinetic *in vivo* will differ from the *in vitro* model. Despite their inhibitory effect, the organic building blocks finally lead to a crack filling of high compositional similarity to human bone. Bone itself consists of apatite and collagen, which profits from its unique hierarchical structure that leads to its outstanding mechanical properties⁵⁸. Therefore, the newly formed material in cracks should perform with superior mechanical properties compared to the man-made implant material. Beyond, CPCs are resorbed *in vivo* and transformed to new bone^{43,59}. During this remodeling process the C-fibers are expected to remain in place and the new bone will be formed around them. Since apatite is only poorly solvable *in vivo*, the remodeling process will take months to years depending on implant size, making the self-healing properties so essential. Due to the small crack openings, associated problems with the ingrowth of blood vessels might occur *in vivo*, which could limit the healing in comparison to *in vitro* conditions⁶⁰. Nevertheless, it is due to the small crack opening that CPCs show damage tolerance, which we suspect to be sufficient for stabilizing the cracks under cyclic loading associated with *in vivo* demands. The increased strength due to the incorporation of both untreated and treated fibers results in sufficient mechanical strength for moderate load bearing applications, e.g. in vertebroplasty. Here, Wilke *et al.* measured compressive loads *in vivo* in the spine in the range of 0.1–2.3 MPa, which is lower than the compressive strength of the α -TCP cement system used in our study^{61,62}.

Conclusion

Self-healing of CPC with respect to the restoration of mechanical properties was achieved, when two key factors, damage tolerance and ion supply are realized simultaneously. Investigation of the crack closing took place for both, extrinsic and intrinsic healing. Intrinsic self-healing requires the presence of calcium and phosphate ions in solution and is therefore solely observed in SBF. Here, bioactive crack area, as well as functionalized C-fibers promote the nucleation of apatite. An extrinsic healing by the NaH_2PO_4 capsules is assumed, since a healing of cements with capsules is also observed in demineralized water. The release of H_2PO_4 from the capsules leads to local supersaturation and thus to mineralization within the cracks. In both cases the mineralization leads to effective change of crack opening and even crack closing, whereby mechanical properties are restored. Due to self-healing over three cycles, a high repeatability can be assumed. This offers new fields of application for the class of CPC, also potentially in load-bearing areas.

Received: 27 February 2020; Accepted: 15 May 2020;

Published online: 10 June 2020

References

1. Van der Zwaag, S. *Self Healing Materials: An Alternative Approach to 20 Centuries of Materials Science*. (Springer, <https://doi.org/10.1007/978-1-4020-6250-6> (2007).
2. Raggatt, L. J. & Partridge, N. C. Cellular and Molecular Mechanisms of Bone Remodeling. *J. Biol. Chem.* **285**, 25103–25108, <https://doi.org/10.1074/jbc.R109.041087> (2010).
3. Henriksen, K., Neutzsky-Wulff, A. V., Bonewald, L. F. & Karsdal, M. A. Local Communication on and within Bone Controls Bone Remodeling. *Bone* **44**, 1026–1033, <https://doi.org/10.1016/j.bone.2009.03.671> (2009).
4. Wool, D. Y., Meure, S. & Solomon, D. Self-Healing Polymeric Materials: A Review of Recent Developments. *Prog. Polym. Sci.* **33**, 479–522, <https://doi.org/10.1016/j.progpolymsci.2008.02.001> (2008).
5. Hager, M. D., Greil, P., Leyens, C., van der Zwaag, S. & Schubert, U. S. Self-Healing Materials. *Adv. Mater.* **22**, 5424–5430, <https://doi.org/10.1002/adma.201003036> (2010).
6. Ghosh, S. K. *Self-Healing Materials: Fundamentals, Design Strategies, and Applications*. (Wiley (2009).
7. Wu, D. Y., Meure, S. & Solomon, D. Self-Healing Polymeric Materials: A Review of Recent Developments. *Prog. Polym. Sci.* **33**, 479–522, <https://doi.org/10.1016/j.progpolymsci.2008.02.001> (2008).
8. Murphy, E. B. & Wudl, F. The World of Smart Healable Materials. *Prog. Polym. Sci.* **35**, 223–251, <https://doi.org/10.1016/j.progpolymsci.2009.10.006> (2010).
9. Brochu, A. B. W., Craig, S. L. & Reichert, W. M. Self-Healing Biomaterials. *J. Biomed. Mater. Res. A* **96**, 492–506, <https://doi.org/10.1002/jbm.a.32987> (2011).
10. Thakur, V. K. & Kessler, M. R. Self-Healing Polymer Nanocomposite Materials: A Review. *Polymer* **69**, 369–383, <https://doi.org/10.1016/j.polymer.2015.04.086> (2015).

11. Bekas, D. G., Tsirka, K., Baltzis, D. & Paipetis, A. S. Self-Healing Materials: A Review of Advances in Materials, Evaluation, Characterization and Monitoring Techniques. *Composites Part B* **87**, 92–119, <https://doi.org/10.1016/j.compositesb.2015.09.057> (2016).
12. Van Tittelboom, K. *et al.* Comparison of Different Approaches for Self-Healing Concrete in a Large-Scale Lab Test. *Constr. Build. Mater.* **107**, 125–137, <https://doi.org/10.1016/j.conbuildmat.2015.12.186> (2016).
13. Diba, M. *et al.* Self-Healing Biomaterials: From Molecular Concepts to Clinical Applications. *Adv. Mater. Interfaces* **5**, 1800118, <https://doi.org/10.1002/admi.201800118> (2018).
14. Greil, P. Generic Principles of Crack-Healing Ceramics. *J. Adv. Ceram.* **1**, 249–267, <https://doi.org/10.1007/s40145-012-0020-2> (2012).
15. Wu, M., Johannesson, B. & Geiker, M. A Review: Self-Healing in Cementitious Materials and Engineered Cementitious Composite as a Self-Healing Material. *Constr. Build. Mater.* **28**, 571–583, <https://doi.org/10.1016/j.conbuildmat.2011.08.086> (2012).
16. Ferguson, J. B., Schultz, B. F. & Rohatgi, P. K. Self-Healing Metals and Metal Matrix Composites. *JOM* **66**, 866–871, <https://doi.org/10.1007/s11837-014-0912-4> (2014).
17. Bhullar, S. K., Lala, N. L. & Ramkrishna, S. Smart Biomaterials - A Review. *Rev. Adv. Mater. Sci.* **40**, 303–314 (2015).
18. Van Tittelboom, K. & De Belie, N. Self-Healing in Cementitious. *Materials - A Review. Materials* **6**, 2182–2217 (2013).
19. Vijay, K., Murmu, M. & Deo, S. V. Bacteria Based Self Healing Concrete - A Review. *Constr. Build. Mater.* **152**, 1008–1014, <https://doi.org/10.1016/j.conbuildmat.2017.07.040> (2017).
20. Yang, C.-W. & Lui, T.-S. Kinetics of hydrothermal crystallization under saturated steam pressure and the self-healing effect by nanocrystallite for hydroxyapatite coatings. *Acta Biomater.* **5**, 2728–2737, <https://doi.org/10.1016/j.actbio.2009.03.014> (2009).
21. Li, Q. *et al.* A novel bio-inspired bone-mimic self-healing cement paste based on hydroxyapatite formation. *Cem. Concr. Compos.* **104**, 103357, <https://doi.org/10.1016/j.cemconcomp.2019.103357> (2019).
22. Kamerer, D. B., Hirsch, B. E., Snyderman, C. H., Costantino, P. & Friedman, C. D. Hydroxyapatite Cement: A New Method for Achieving Watertight Closure in Transtemporal Surgery. *Am. J. Otol.* **15**, 47–49 (1994).
23. Constantz, B. R. *et al.* Skeletal Repair by in Situ Formation of the Mineral Phase of Bone. *Science* **267**, 1796, <https://doi.org/10.1126/science.7892603> (1995).
24. Brown, W. E. & Chow, L. C. Dental Restorative Cement Pastes. Patent-No. 4518430 (1985).
25. Bohner, M. Calcium Orthophosphates in Medicine: From Ceramics to Calcium Phosphate Cements. *Injury* **31**, D37–D47, [https://doi.org/10.1016/S0020-1383\(00\)80022-4](https://doi.org/10.1016/S0020-1383(00)80022-4) (2000).
26. Fernandez, E. *et al.* Calcium Phosphate Bone Cements for Clinical Applications. Part II: Precipitate Formation During Setting Reactions. *J. Mater. Sci. Mater. Med.* **10**, 177–183, <https://doi.org/10.1023/a:1008989525461> (1999).
27. Bohner, M. Reactivity of Calcium Phosphate Cements. *J. Mater. Chem.* **17**, 3980–3986, <https://doi.org/10.1039/B706411J> (2007).
28. Ginebra, M. P., Traykova, T. & Planell, J. A. Calcium Phosphate Cements as Bone Drug Delivery Systems: A Review. *J. Control. Release* **113**, 102–110, <https://doi.org/10.1016/j.jconrel.2006.04.007> (2006).
29. Bohner, M., Gbureck, U. & Barralet, J. E. Technological Issues for the Development of more Efficient Calcium Phosphate Bone Cements: A Critical Assessment. *Biomaterials* **26**, 6423–6429, <https://doi.org/10.1016/j.biomaterials.2005.03.049> (2005).
30. Canal, C. & Ginebra, M. P. Fibre-Reinforced Calcium Phosphate Cements: A Review. *J. Mech. Behav. Biomed. Mater.* **4**, 1658–1671, <https://doi.org/10.1016/j.jmbbm.2011.06.023> (2011).
31. Dos Santos, L. A. *et al.* Fiber Reinforced Calcium Phosphate Cement. *Artif. Organs* **24**, 212–216, <https://doi.org/10.1046/j.1525-1594.2000.06541.x> (2000).
32. Geffers, M., Groll, J. & Gbureck, U. Reinforcement Strategies for Load-Bearing Calcium Phosphate Biocements. *Materials* **8**, 2700 (2015).
33. Wang, X., Ye, J., Wang, Y. & Chen, L. Reinforcement of Calcium Phosphate Cement by Bio-Mineralized Carbon Nanotube. *J. Am. Ceram. Soc.* **90**, 962–964, <https://doi.org/10.1111/j.1551-2916.2006.01460.x> (2007).
34. Zorn, K., Vorndran, E., Gbureck, U. & Müller, F. A. Reinforcement of a Magnesium-Ammonium-Phosphate Cement with Calcium Phosphate Whiskers. *J. Am. Ceram. Soc.* **98**, 4028–4035, <https://doi.org/10.1111/jace.13858> (2015).
35. Boehm, A. V., Meiningner, S., Tesch, A., Gbureck, U. & Müller, F. A. The Mechanical Properties of Biocompatible Apatite Bone Cement Reinforced with Chemically Activated Carbon Fibers. *Materials* **11**, 192 (2018).
36. Xu, H. H. K., Eichmiller, F. C. & Barndt, P. R. Effects of Fiber Length and Volume Fraction on the Reinforcement of Calcium Phosphate Cement. *J. Mater. Sci. Mater. Med.* **12**, 57–65, <https://doi.org/10.1023/A:1026753020208> (2001).
37. Xu, H. H. K., Eichmiller, F. C. & Giuseppetti, A. A. Reinforcement of a Self-Setting Calcium Phosphate Cement with Different Fibers. *J. Biomed. Mater. Res.* **52**, 107–114, [10.1002/1097-4636\(200010\)52:1<107::AID-JBM13>3.0.CO;2-0](https://doi.org/10.1002/1097-4636(200010)52:1<107::AID-JBM13>3.0.CO;2-0) (2000).
38. Müller, L. & Müller, F. A. Preparation of SBF with Different HCO³⁻ Content and its Influence on the Composition of Biomimetic Apatites. *Acta Biomater.* **2**, 181–189 (2006).
39. Oyane, A. *et al.* Preparation and Assessment of Revised Simulated Body Fluids. *J. Biomed. Mater. Res. A* **65A**, 188–195, <https://doi.org/10.1002/jbm.a.10482> (2003).
40. Filgueiras, M. R., La Torre, G. & Hench, L. L. Solution Effects on the Surface Reactions of a Bioactive Glass. *J. Biomed. Mater. Res.* **27**, 445–453, <https://doi.org/10.1002/jbm.820270405> (1993).
41. Kokubo, T. & Takadama, H. How Useful is SBF in Predicting in Vivo Bone Bioactivity? *Biomaterials* **27**, 2907–2915, <https://doi.org/10.1016/j.biomaterials.2006.01.017> (2006).
42. Kokubo, T. Bioactive Glass Ceramics: Properties and Applications. *Biomaterials* **12**, 155–163, [https://doi.org/10.1016/0142-9612\(91\)90194-F](https://doi.org/10.1016/0142-9612(91)90194-F) (1991).
43. Kanter, B., Geffers, M., Ignatius, A. & Gbureck, U. Control of in Vivo Mineral Bone Cement Degradation. *Acta Biomater.* **10**, 3279–3287, <https://doi.org/10.1016/j.actbio.2014.04.020> (2014).
44. Currey, J. D. Physical Characteristics Affecting the Tensile Failure Properties of Compact Bone. *J. Biomech.* **23**, 837–844, [https://doi.org/10.1016/0021-9290\(90\)90030-7](https://doi.org/10.1016/0021-9290(90)90030-7) (1990).
45. Fernández, E. *et al.* Improvement of the Mechanical Properties of New Calcium Phosphate Bone Cements in the CaHPO₄-α-Ca₃(PO₄)₂ System: Compressive Strength and Microstructural Development. *J. Biomed. Mater. Res.* **41**, 560–567, [10.1002/\(sici\)1097-4636\(19980915\)41:4<560::Aid-jbm7>3.0.Co;2-a](https://doi.org/10.1002/(sici)1097-4636(19980915)41:4<560::Aid-jbm7>3.0.Co;2-a) (1998).
46. Prakash, K. H., Kumar, R., Yu, S. C., Khor, K. A. & Cheang, P. On the Kinetics of Apatite Growth on Substrates under Physiological Conditions. *Langmuir* **22**, 269–276, <https://doi.org/10.1021/la0522348> (2006).
47. Dey, A. *et al.* The Role of Prenucleation Clusters in Surface-Induced Calcium Phosphate Crystallization. *Nat. Mater.* **9**, 1010, <https://doi.org/10.1038/nmat2900> <https://www.nature.com/articles/nmat2900#supplementary-information> (2010).
48. Müller, F. A., Müller, L., Caillard, D. & Conforto, E. Preferred Growth Orientation of Biomimetic Apatite Crystals. *J. Cryst. Growth* **304**, 464–471, <https://doi.org/10.1016/j.jcrysgro.2007.03.014> (2007).
49. Radin, S. R. & Ducheyne, P. The effect of calcium phosphate ceramic composition and structure on in vitro behavior. II. *Precipitation. J. Biomed. Mater. Res.* **27**, 35–45, <https://doi.org/10.1002/jbm.820270106> (1993).
50. Chen, X., Lei, B., Wang, Y. & Zhao, N. Morphological control and in vitro bioactivity of nanoscale bioactive glasses. *J. Non-Cryst. Solids* **355**, 791–796, <https://doi.org/10.1016/j.jnoncrysol.2009.02.005> (2009).
51. Siriphannon, P., Kameshima, Y., Yasumori, A., Okada, K. & Hayashi, S. Comparative study of the formation of hydroxyapatite in simulated body fluid under static and flowing systems. *J. Biomed. Mater. Res.* **60**, 175–185, <https://doi.org/10.1002/jbm.10056> (2002).

52. Griffith, A. A. & Taylor, G. I. V. I. The phenomena of rupture and flow in solids. *Philosophical Transactions of the Royal Society of London. Series A, Containing Papers of a Mathematical or Physical Character* **221**, 163–198, <https://doi.org/10.1098/rsta.1921.0006> (1921).
53. Faber, K. T. & Evans, A. G. Crack Deflection Processes - I. Theory. *Acta Metall.* **31**, 565–576, [https://doi.org/10.1016/0001-6160\(83\)90046-9](https://doi.org/10.1016/0001-6160(83)90046-9) (1983).
54. Faber, K. T. & Evans, A. G. Crack Deflection Processes - II. Experiment. *Acta Metall.* **31**, 577–584, [https://doi.org/10.1016/0001-6160\(83\)90047-0](https://doi.org/10.1016/0001-6160(83)90047-0) (1983).
55. Kim, H.-M., Himeno, T., Kawashita, M., Kokubo, T. & Nakamura, T. The Mechanism of Biomineralization of Bone-Like Apatite on Synthetic Hydroxyapatite: An in Vitro Assessment. *J. Royal Soc. Interface* **1**, 17–22, <https://doi.org/10.1098/rsif.2004.0003> (2004).
56. Oliveira, A. L., Costa, S. A., Sousa, R. A. & Reis, R. L. Nucleation and Growth of Biomimetic Apatite Layers on 3D Plotted Biodegradable Polymeric Scaffolds: Effect of Static and Dynamic Coating Conditions. *Acta Biomater.* **5**, 1626–1638, <https://doi.org/10.1016/j.actbio.2008.12.009> (2009).
57. Termine, J. D., Eanes, E. D. & Conn, K. M. Phosphoprotein Modulation of Apatite Crystallization. *Calcif. Tissue Int.* **31**, 247–251, <https://doi.org/10.1007/bf02407188> (1980).
58. Launey, M. E., Buehler, M. J. & Ritchie, R. O. On the Mechanistic Origins of Toughness in Bone. *Annu. Rev. Mater. Res.* **40**, 25–53, <https://doi.org/10.1146/annurev-matsci-070909-104427> (2010).
59. Sheikh, Z. *et al.* Mechanisms of in Vivo Degradation and Resorption of Calcium Phosphate Based Biomaterials. *Materials* **8**, 7913–7925 (2015).
60. Malhotra, A. & Habibovic, P. Calcium Phosphates and Angiogenesis: Implications and Advances for Bone Regeneration. *Trends Biotechnol.* **34**, 983–992, <https://doi.org/10.1016/j.tibtech.2016.07.005> (2016).
61. Wilke, H. J., Neef, P., Caimi, M., Hoogland, T. & Claes, L. E. New *In Vivo* Measurements of Pressures in the Intervertebral Disc in Daily Life. *Spine (Phila Pa 1976)* **24**, 755–762 (1999).
62. Gbureck, U., Spatz, K., Thull, R. & Barralet, J. E. Rheological enhancement of mechanically activated α -tricalcium phosphate cements. *Journal of Biomedical Materials Research Part B: Applied Biomaterials* **73B**, 1–6, <https://doi.org/10.1002/jbm.b.30148> (2005).

Acknowledgements

The SEM facilities of the Jena Center for Soft Matter (JCSM) were established with a grant from the Deutsche Forschungsgemeinschaft (DFG). Furthermore, the authors would like to acknowledge the facilities offered for fluidized bed coating at the Chair of Pharmaceutics and Biopharmacy (Prof. Dr. Dr. Lorenz Meinel) at the University of Würzburg. The authors thank the DFG for financial support of project MU1803/16–1 and GB1/21-1.

Author contributions

A.V.B. performed CPC preparation, mechanical experiments and self-healing tests. S.M. performed the capsule preparation. U.G. developed and prepared the cement raw powder. A.V.B., S.M., U.G. and F.A.M. wrote the paper. All authors significantly contributed in discussing the results.

Competing interests

The authors declare no competing interests.

Additional information

Correspondence and requests for materials should be addressed to F.A.M.

Reprints and permissions information is available at www.nature.com/reprints.

Publisher's note Springer Nature remains neutral with regard to jurisdictional claims in published maps and institutional affiliations.



Open Access This article is licensed under a Creative Commons Attribution 4.0 International License, which permits use, sharing, adaptation, distribution and reproduction in any medium or format, as long as you give appropriate credit to the original author(s) and the source, provide a link to the Creative Commons license, and indicate if changes were made. The images or other third party material in this article are included in the article's Creative Commons license, unless indicated otherwise in a credit line to the material. If material is not included in the article's Creative Commons license and your intended use is not permitted by statutory regulation or exceeds the permitted use, you will need to obtain permission directly from the copyright holder. To view a copy of this license, visit <http://creativecommons.org/licenses/by/4.0/>.

© The Author(s) 2020